HHS Public Access

Author manuscript

Acta Biomater. Author manuscript; available in PMC 2019 December 01.

Published in final edited form as:

Acta Biomater. 2018 December ; 82: 1–11. doi:10.1016/j.actbio.2018.10.016.

Pore Size Directs Bone Marrow Stromal Cell Fate and Tissue Regeneration in Nanofibrous Macroporous Scaffolds by Mediating Vascularization

Melanie J. Gupte[#a], **W. Benton Swanson**[#b], **Jiang H**[b], **Xiaobing Jin**[b], **Haiyun Ma**[b], **Zhanpeng Zhang**[a], **Zhongning Li**[b], **Kai Feng**[b,c], **Ganjun Feng**[b], **Guiyong Xiao**[b], **Nan Hatch**[e], **Yuji Mishina**[b], and **Peter X. Ma**[a,b,c,d,*]

[a]Department of Biomedical Engineering, College of Engineering, University of Michigan, 2200 Bonisteel Blvd, Ann Arbor, MI, USA 48109

[b]Department of Biologic and Materials Science, School of Dentistry, University of Michigan, 1011 N University Ave, Ann Arbor, MI, USA 48109

[c]Department of Materials Science and Engineering, College of Engineering, University of Michigan, 2300 Hayward St, Ann Arbor, MI, USA 48109

[d]Macromolecular Science and Engineering Center, College of Engineering, University of Michigan, 2300 Hayward St, Ann Arbor, MI, USA 48109

[e]Department of Orthodontics and Pediatric Dentistry, School of Dentistry, University of Michigan, 1011 N University Ave, Ann Arbor, MI, USA 48109

[#] These authors contributed equally to this work.

Abstract

In the U.S., 30% of adults suffer joint pain, most commonly in the knee, which severely limits mobility and is often attributed to injury of cartilage and underlying bone in the joint. Current treatment methods such as microfracture result in less resilient fibrocartilage with eventual failure; autografting can cause donor site morbidity and poor integration. To overcome drawbacks in treatment, tissue engineers can design cell-instructive biomimetic scaffolds using biocompatible materials as alternate therapies for osteochondral defects. Nanofibrous poly (L-lactic acid) (PLLA) scaffolds of uniform, spherical, interconnected and well-defined pore sizes that are fabricated using a thermally-induced phase separation and sugar porogen template method create an extracellular matrix-like environment which facilitates cell adhesion and proliferation. Herein we report that chondrogenesis and endochondral ossification of rabbit and human bone marrow

[*]Corresponding Author: **Prof. Peter X. Ma**, mapx@umich.edu, Telephone: +1 734-764-2209, Fax: +1 734-647-2805, Department of Biologic and Materials Science, School of Dentistry, University of Michigan, 1011 N University Ave, Rm 2208, Ann Arbor, MI, USA 48109.

Disclosures

The authors declare no competing interests.

stromal cells (BMSCs) can be controlled by scaffold pore architecture, particularly pore size. Small-pore scaffolds support enhanced chondrogenic differentiation *in vitro* and cartilage formation *in vivo* compared to large-pore scaffolds. Endochondral ossification is prevented in scaffolds with very small pore sizes; pore interconnectivity is critical to promote capillary ingrowth for mature bone formation. These results provide a novel strategy to control tissue regenerative processes by tunable architecture of macroporous nanofibrous scaffolds.

Graphical Abstract

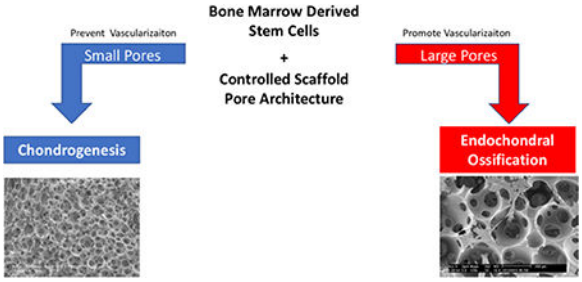

Keywords

pore size; vascularization; bone marrow stromal cells; bone tissue engineering; cartilage tissue engineering

1. Introduction

Osteochondral defects are common in humans. In a study of 1,000 knee arthroscopies for pain and/or injury, over 60% of patients had a chondral or osteochondral lesion [1]. Osteochondral defects are also common in athletes due to repeated stresses placed on the joints during physical activity [2], causing cartilage volume to decrease. Resulting osteochondral defects have limited capability of self-repair. If articular cartilage further degenerates, osteoarthritis develops [3]. Currently, there are two treatment options for small osteochondral defects: microfracture and autografts [4]. While microfracture can relieve pain, the resulting fibrocartilage does not have the same resiliency of articular cartilage and can fail over time [3]. Autografts require multiple surgeries, are difficult to match defect geometry, and can cause donor site morbidity [5]. Due to the significant drawbacks of current treatment options, there is a clear need for an alternate therapy such as a tissue-engineered osteochondral graft.

In cartilage and bone tissue engineering, scaffolds play a critical role by serving as an artificial extracellular matrix (ECM) [6, 7]. Our laboratory has developed a novel method using thermally induced phase separation (TIPS) to produce a synthetic biodegradable polymer scaffold with a nanofibrous (NF) structure. Poly(l-lactic acid) (PLLA) is phase separated from tetrahydrofuran (THF) solvent at a low temperature [8]; the resulting nanofibers range from 50 to 500 nm in diameter. TIPS-generated nanofibers facilitate tissue regeneration by mimicking the size of collagen fibers in the native ECM [9]. THF is chosen as solvent because of its ability to form nanofibers quickly and at reasonable temperatures

[8]. The nanofibers have been demonstrated to promote cell adhesion, proliferation, differentiation, and tissue neogenesis of multiple stem cell types [10–12].

Ideally, scaffolds should have an internal interconnected porous network which facilitates cellular integration, uniform cell distribution, vascularization, and nutrient/waste exchange [13]. Porous scaffolds have two key design parameters: pore size and pore interconnectivity. Porous structures are shown to allow vascularization in synthetic membranes [18], chitosan scaffolds [19], and PEG hydrogels [20]. Literature suggests a recommended a pore size greater than 300 μm for bone formation and capillary ingrowth [14]. Others have characterized pore size and stem-cell differentiation relationships in dental pulp stem cells [15] and vascular smooth muscle cells [16]. However, pore architecture varies greatly between scaffold systems [17]. For example, scaffolds fabricated by salt leaching [21] or gas foaming [22] methods have resulted in minimal interconnectivity which precludes uniform cell penetration and mass transport; uniformly spherical porogen particles are advantageous in controlling pore interconnectivity [23–26]. We have previously shown that scaffolds fabricated from a sugar porogen template have uniform, spherical, well-interconnected pores with intricate control over pore size and interconnectivity, and without residue on the scaffold walls after porogen leaching [27–29]. This fabrication method can be combined with TIPS to induce nanofiber formation; the combination is a good model for investigating how scaffold pore size controls cell differentiation.

The regenerative capacity of damaged or osteoarthritic articular cartilage is limited due to the avascularity of cartilage and low mitotic activity of chondrocytes [30]. Bone-marrow stromal cells (BMSCs) are a suitable cell source because of their differentiation capacity and are easily be isolated from a patient’s bone marrow, making their use clinically translatable.

Chondrogenesis of BMSCs involved four key steps: mesenchymal condensation, chondrogenic commitment, differentiation into chondrocytes, and secretion of ECM. The initial step, mesenchymal condensation, involves the formation of a dense three-dimensional mesenchymal progenitor/stem cell (MSC) aggregate [31–33]. Thus, a scaffold that facilitates aggregation and BMSC condensation is desirable to guide cartilage regeneration. The complex and tunable architectural features of our NF scaffold, previously shown to promote chondrogenic differentiation of human BMSCs (hBMSCs) [12], lends a greater control of the cell microenvironment compared to commonly used hydrogels [34]. In this study we compare the chondrogenic differentiation of hBMSCs on NF scaffolds with two distinct pore sizes both *in vitro,* and *in vivo* in a mouse subcutaneous implantation model.

Unlike cartilage, bone is a highly vascularized tissue comprised of a collagen type I-rich matrix that is mineralized with hydroxyapatite. During development and healing, long bone is formed via endochondral ossification, where a cartilage matrix template is followed by blood vessel invasion, carrying osteoprogenitor cells [35]. However, this native bone healing is not sufficient to repair critical-sized bone defects on its own, calling for a tissue-engineered bone graft that supports endochondral ossification [6]. Bone tissue-engineering scaffolds are often made of ceramic-like hydroxyapatite or β-tricalcium phosphate due to their osteoconductivity [36]. While ceramics have proven effective for bone regeneration, they do not support cartilage formation [24, 37]. On the other hand, nanofibrous scaffolds

are conductive to both cartilage and bone formation [12, 38, 39]. Biodegradable synthetic polymer scaffolds are desirable due to their high processability and easily tailored design features, including a porous network [27, 40, 41]. A nanofibrous (NF) structure is analogous structure to abundant collagen in the ECM, and conductive to cell proliferation and attachment. A highly porous, phase-separated NF polymer scaffold with uniform, interconnected spherical pore structure is a good model to examine the effect of pore size on stem cell differentiation. The importance of vascularization in tissue neogenesis is known [42]; methods of modulating vascularization using physical cues in a controlled PLLA scaffold architecture are not described. How the fate of mesenchymal progenitor/stem cells is affected by the physical cues are not well understood. We hypothesized that small pores are necessary to facilitate cartilage neogenesis, by preventing vascular ingrowth in vivo in order to maintain avascularity and prevent endochondral ossification. Additionally, we hypothesized that the larger well-interconnected macro-pores will facilitate endochondral ossification by allowing blood vessel in-growth. By tailoring the pore size of this novel synthetic material, we believe that BMSC-seeded, nanofibrous scaffolds with optimized pore size can direct both chondrogenesis and endochondral ossification processes, by modulating vascularization, towards cartilage and bone tissue that recapitulates the native physiological properties.

2. Materials and Methods

2.1 Materials

D-fructose was purchased from VWR (Radnor, PA). Span80®, tetrahydrofuran (THF), mineral oil, Triton-X, phosphate buffered saline (PBS, pH 7.4), papain solution, dimethylmethylene blue, shark chondroitin 4-sulfate, Alcian blue, and Safranin-O were purchased from Sigma-Aldrich (Milwaukee, WI). Poly (L-lactic acid) (PLLA, Resomer L207S) with an inherent viscosity of 1.6 dL/g was purchased from Boehringer Ingelheim (Ingelheim, Germany). Hexane, cyclohexane, formaldehyde, heparin-containing maintenance media (high-glucose alpha-MEM (Gibco), fetal bovine serum (FBS) (Gibco) and antibiotics (penicillin G, 100 U/mL; streptomycin, 0.1 mg/mL)), chondrogenic growth medium, Alexa-Fluor® 555 phalloidin (#A34055), hematoxylin and eosin stains, pepsin, collagen type II antibody, 200 proof ethanol, and Invitrogen Ultrapure (TM) Agarose was purchased from ThermoFischer (Fremont, CA). MSC Growth Medium was purchased from Lonza (Allendale, NJ). TGF-β1 was purchased from Peprotech (Rocky Hill, NJ). DAPI was purchased from Vector Laboratories (Burlingame, CA). Tissue-Tearor was purchased from BioSpec Products, Inc. (Bartlesville, OK). TaqMan reverse transcription reagents, TaqMan Universal PCR Master Mix, pre-designed primers and probes were purchased from Applied Biosystems (Foster City, CA). Cell & Tissue Staining Kit was purchased from R&D systems Inc. (Minneapolis, MN). CD31 antibody was purchased from Abcam (Cambridge, MA). RNeasy Mini Kit was purchased from Qiagen (Valencia, CA). Bone marrow stromal cells (BMSCs) were isolated from New Zealand white rabbits in our laboratory. Human bone marrow stromal cells (hMSCs) were obtained from Lonza Walkersville, Inc. (Walkersville, MD). All reagents were used as received unless otherwise noted.

2.2 Fabrication of NF PLLA scaffolds with different pore sizes

Fabrication of three-dimensional nanofibrous (NF) scaffolds has been described in detail previously [27]. Sugar spheres of different sizes were first prepared by an emulsion technique. D-fructose (50 g) was melted at 120°C for 90 min until clear yellowish liquid was obtained. The liquefied sugar was emulsified into mineral oil (50 mL) with Span80® (1.3 mL) at 120°C under fast stirring. The resulting mixture was cooled using an ice-bath to solidify sugar spheres. The sugar spheres were washed with hexane three times to remove the mineral oil, and sieved to separate desired size ranges (60–125, 125–250, 250–425, and 425–600 μm). The sieved sugar spheres were packed in a Teflon vial with hexane and heat treated at 37°C to achieve an interconnected sugar sphere template. After bonding, excess hexane was removed and the sugar template was dried under vacuum. A PLLA/THF (10% w/v) solution was cast into an assembled sugar template under mild vacuum. The polymer-sugar composite was phase separated at −20°C overnight, then immersed into cyclohexane to exchange THF for two days. The composites were lyophilized, then the sugar template was leached in distilled water and lyophilized again to obtain highly porous scaffolds. Scaffolds were cut to 3.6 mm in diameter and 1 mm in thickness. For cell culture studies, the scaffolds were sterilized with ethylene oxide.

2.3 SEM characterization of scaffolds

Scaffolds were sputter-coated with gold for 120 s (DeskII, Denton Vacuum, Inc.) and observed under a scanning electron microscope (Philips XL30 FEG) at 10 kV. Quantification of interconnection opening size and ratio followed the method of a previous report [27] using scanning electron microscopy (SEM) micrographs and ImageJ software (NIH, Bethesda, MD). At least 10 pores for each type of scaffold were selected for analysis.

2.4 hBMSC seeding and culture on scaffolds

hBMSCs were cultured according to the manual provided by the supplier. Scaffolds were soaked in ethanol (70%) for 30 min to increase their hydrophilicity, washed three times with PBS for 30 min each, then soaked twice in Lonza's MSC Growth Medium for 2 hours each on an orbital shaker at 75 rpm. 2.5×10^5 cells were seeded onto each scaffold (3.6 mm diameter, 1 mm thickness). After 2 hours of initial seeding, cell-seeded scaffolds were further cultured for 22 hours under static condition to enhance cell adhesion on scaffolds. To induce chondrogenesis, cell-seeded scaffolds were transferred to 15 mL polypropylene culture tubes and maintained in chondrogenic medium (0.5 mL; DMEM, 1% insulin-transferrin-selenium (Gibco ITS-G 100× diluted by a factor of 100), 100 μg/mL sodium pyruvate, 40 μg/mL proline, 10^{-7} M dexamethasone, 50μg/mL ascorbic acid) supplemented with TGF-β1 (10 ng/mL). The medium was changed every 2–3 days.

2.5 rBMSC isolation and culture

Bone marrow stromal cells (BMSCs) were obtained from New Zealand White rabbits by aspiration of the femoral and tibial bone marrow using an 18-gauge syringe needle. A total of 10 mL of marrow was collected into 1000 U of heparin-containing maintenance media (high-glucose alpha-MEM containing 10% fetal bovine serum (FBS) and antibiotics (100 U/mL penicillin G; 0.1 mg/mL streptomycin)). The marrow was washed with PBS once and

fresh media twice, centrifuged at 2000 rpm for 3 min after each wash. Rabbit BMSCs were collected and cultured in 60 cm^2 culture dishes in maintenance media at 37°C under 5% CO_2, changing media every 2–3 days. Cells were used at passage 3. rBMSCs are used in in vivo experiments because they are easily isolated in large quantities.

2.6 BMSC seeding and culture on scaffolds

Scaffolds were soaked in 70% ethanol for 30 min, washed three times with PBS for 30 min each, then soaked twice in alpha MEM (supplemented with 10% fetal bovine serum) for 30 min each. 12 uL of media containing 2.5×10^5 cells (2×10^7 cells/mL concentration) were seeded onto each scaffold (3.6 mm diameter, 1.5 mm thickness) in an untreated (hydrophobic) culture plate. After 2 hours of initial seeding, media was added to cover cell-seeded scaffolds, which were further cultured for 22 hours under static condition to enhance cell adhesion and promote cell spreading. The constructs were transferred to 6-well tissue culture plates, and cultured on an orbital shaker at 75 rpm in a humidified incubator. Cell attachment to scaffolds is assessed by DNA quantification (Method 2.8).

2.7 Immunofluorescent staining

After 24 hours, constructs were washed in PBS and fixed in formaldehyde (4%) for 1 hour. Cell membranes were then permeabilized in Triton-X (0.1%) for 5 min. After washing in PBS three times, the actin cytoskeleton was stained using Alexa-Fluor® 555 phalloidin (1:35 dilution) in bovine serum albumin (1%) as specified by the manufacturer. Constructs were mounted on slides in mounting media containing DAPI and observed using confocal microscopy (Nikon Eclipse C1). n=3 per group.

2.8 Total DNA quantification

After 24 hours of initial seeding and culture, the constructs were washed with PBS for 5 min, homogenized with a Tissue-Tearor, and the DNA content was determined with the DNA Quantification Fluorescence Assay Kit from Sigma. n=3 for each group.

2.9 Gene expression analysis

Samples were homogenized with a Tissue-Tearer. Total RNA was isolated using RNeasy Mini Kit according to the manufacturer's protocol. cDNA was reverse-transcribed with TaqMan reverse transcription reagents. Real time PCR ($n \geq 3$ per group) was carried out using TaqMan Universal PCR Master Mix and pre-designed primers and probes for collagen type I (Hs00164004_m1), collagen type II (Hs01064869_m1) on a ViiA 7 Real time PCR system (Applied Biosystems). The gene expression level was normalized against glyceraldehyde 3phosphate dehydrogenase (GAPDH, Hs99999905_m1) expression. n=3 for each group.

2.10 Glycosaminoglycan (GAG) assay

GAG amount was quantified according to a previously published method [43]. Briefly, constructs were harvested after 2 and 4 weeks of culture, and washed with PBS before digest with 100 μL papain solution (280 μg/mL in 50 mM sodium phosphate, pH 6.5, containing 5 mM *N*-acetyl cysteine and 50 mM EDTA) for 24 hr. at 65°C. GAG content was determined

by reaction with dimethylmethylene blue. Optical density was measured at 525 nm and GAG content was calculated against a shark chondroitin 4-sulfate standard calibration (Hitachi U-2910 spectrometer). n=3 per group.

2.11 Subcutaneous implantation in mice

Following induction *in vitro*, cell-scaffold constructs were implanted subcutaneously into nude mice for 4 or 8 weeks. Male nude mice that were 6–8 weeks old (Charles River, Wilmington, MA) were used. Surgery was performed under general anesthesia by inhalation of isoflurane (with balanced oxygen). To implant four constructs per mouse, two midsagittal incisions were made on the dorsa, and one subcutaneous pocket was created on each side of each incision. One cell-scaffold construct was implanted into each pocket at random. Four samples were implanted for each group (different pore size). Incisions were closed with suture clips. Following 4 or 8week implantation period, mice were euthanized with CO_2 and implants harvested. These animal procedures were performed according to a protocol approved by the University Committee on Use and Care of Animals (UCUCA) at the University of Michigan and National Institutes of Health guidelines for the care and use of laboratory animals. n=3 per group.

2.12 Histological analysis

Constructs were washed in PBS and fixed with 3.7% formaldehyde in PBS overnight. Where appropriate, samples were decalcified in 10% EDTA (pH=7.4) for two weeks. Constructs were dehydrated through a graded series of ethanol, embedded in paraffin, and sectioned at a thickness of 5 μm. For histological analysis, sections were deparaffinized, rehydrated, and stained with H&E, Alcian blue or Safranin-O. For immunohistochemical staining of cartilage samples, rehydrated sections were pre-treated with pepsin solution for 15 min, incubated with a collagen type II antibody at 1:100 dilution for 1 hr. and detected by a Cell & Tissue Staining Kit according to the manual. All sections were counterstained with hematoxylin. For immunohistochemical staining of bone samples, rehydrated sections were heated to 99°C for 10 min in citrate buffer for heat-induced antigen retrieval, and blocked using the Cell & Tissue Staining Kit, according to the manual. Slides were then incubated with CD31 endothelial cell marker antibody at 1:50 dilution overnight, detected by the kit's AEC chromogen, and counterstained with hematoxylin. n=3 per group, per analysis.

2.13 Micro CT analysis

Samples were embedded in 1% agarose and placed in a 14 mm diameter tube and scanned over the entire length of the scaffold using a microCT system (Scanco μCT 100, Bassersdorf, Switzerland). Scan settings were: voxel size 12 μm, 70 kVp, 114 μA, 0.5 mm AL filter, and integration time 500 ms. Analysis was performed using Scanco MicroCT evaluation and reconstruction software, and a fixed global threshold of 18% (180 on a grayscale of 0–1,000) was used to segment bone from non-bone to in order to quantify bone volume (absolute, mm^3) and create 3D reconstructions. n=3 per group, per time point.

2.14 Statistical Methods

For cell culture studies, numerical values were reported as mean ± standard deviation (n=3). To test the significance of observed differences between the study groups, the Student's t-test was applied. A value of $p<0.05$ was considered to be statistically significant. Analysis of bone volume results was performed using ANOVA followed by a post-hoc Tukey test in JMP Pro 11 (by SAS).

3. Results

3.1 Scaffold architecture is well controlled by sugar sphere porogen.

Four scaffold pore size ranges (60–125, 125–250, 250–425, and 425–600 μm) generated using a sugar sphere templating technique that we developed [27] were used to study the effect of pore size on BMSC differentiation, both in vitro and in vivo. The pores were quite uniform, spherical, and well-interconnected as shown by scanning electron microscopy micrographs (SEM) (Figure 1A). Scaffolds of each pore size have similar NF matrix microstructures that mimic the native ECM, as a result of the TIPS fabrication method (Figure 1B).

3.2 Scaffold pore size does not affect cell infiltration.

After 24 hours of initial seeding and culture, human bone marrow stromal cells (hBMSCs) formed aggregates inside the small-pore (125–250 μm) and large-pore (425–600 μm) scaffolds as shown by immunofluorescence of F-actin in representative confocal images (red, Figure 2A-B). The size of aggregates was confined by the pore size with fewer cells in the aggregates within small pores compared to large pores. There was no significant difference in total DNA amount 24 hours after cell seeding, demonstrating comparable seeding efficiency on both small and large-pore scaffolds (Figure 2C).

3.3 Molecular and histological analyses of chondrogenic fate of hBMSCs *in vitro*

Glycosaminoglycan (GAG) content was quantified for cell-scaffold constructs cultured *in vitro* for 2 and 4 weeks. A significantly higher amount of GAG was secreted by cells cultured on small-pore (125–250 μm) scaffolds than cells cultured on large-pore (425–600 μm) scaffolds during the two culture periods. GAG deposition into scaffolds increased with time for both pore sizes (Figure 3A). Total RNA was extracted from constructs and subjected to gene expression analyses after 2 weeks. Collagen type II gene expression was significantly higher in small-pore than large-pore constructs (Figure 3B); conversely, collagen type I gene expression levels were significantly lower in small-pore compared to large-pore constructs (Figure 3C).After 4 weeks of culture, the constructs were subjected to histological analysis. hBMSCs grew similarly throughout both the small (Figure 4A) and large-pore scaffolds (Figure 4B) during the culture period, shown by H&E staining. Consistent with GAG quantification data, a denser GAG-containing ECM was deposited in small (Figure 4C) compared to large-pore scaffolds (Figure 4D), as indicated by Alcian blue staining of GAG. Immunohistological staining showed a greater amount of collagen type II (brown) deposited into the ECM by cells cultured in small (Figure 4E) as compared to large-pore scaffolds (Figure 4F), also consistent with gene expression results.

3.4 Histological analyses of chondrogenic fate of hBMSCs *in vivo*

Following 4 weeks in vitro chondrogenic culture and subsequent 8 weeks of in vivo mouse subcutaneous implantation, small-pore (125–250 μm) implants supported cartilage formation with typical cartilage morphology such as the spherical cell shape and characteristic lacunae structure (Figure 5A). In contrast, large-pore (400–625 μm) implants did not maintain the chondrogenic phenotype and show blood vessel ingrowth (Figure 5B). Safranin-O staining demonstrated the presence of GAG in small (Figure 5C), but not in large-pore (Figure 5D) constructs indicated by the orange staining. Immunohistological staining for endothelial cell marker CD31 (for blood vessel visualization) showed that small-pore implants were mostly avascular cartilage tissue (Figure 5E), while large-pore implants contained rich microvessels (Figure 5F).

3.5 MicroCT analyses of rBMSC-implant bone volume *in vivo*

Scaffolds of each pore size (60–125, 125–250, 250–425, and 425–600 μm) were seeded with rabbit bone marrow stromal cells (rBMSCs) and implanted subcutaneously into nude mice to evaluate bone formation in an ectopic model. Following 4 and 8 weeks *in vivo*, bone volumes of the constructs were quantified from MicroCT data. After 4 weeks, bone volume increased with increasing pore size, but the increase was not statistically significant. After 8 weeks of subcutaneous implantation, the large pore scaffold (425–600 μm) had significantly higher bone volume than the very small pore scaffold (60–125 μm). There is a clear trend that bone volume increases with increasing pore size (Figure 6A).

MicroCT data was used to create 3D reconstructions of the 8-week explanted constructs from the top and side cross-section views (Figure 6B-E). From the top view, robust bone formation occurred on the outside of all four pore size scaffolds, because the edges of the scaffolds are easily vascularized in the subcutaneous space. Additionally, all constructs held their original, disc-like shape likely as cartilage tissue quickly filled the porous scaffold, providing enough mechanical integrity to withstand the force placed on the scaffold *in vivo*. From the side cross-sectional view of the constructs, the small (125–250 μm), medium (250–425 μm), and large (425600 μm) pore scaffolds contained uniform bone formation throughout the entire cross-section. Bone volume increased with increasing pore size. In contrary, the very small pore scaffold (60125 μm) did not accommodate bone formation throughout the entire cross-section, instead bone formation was only observed on the outer shell of the construct. The small and medium-pore scaffolds facilitated a similar amount of bone formation on the pore walls, while the large pore scaffold had thicker layer bone matrix on the pore walls, though not significantly higher bone volume than small or medium pore scaffolds (Figure 6A).

3.6 Histological analyses of rBMSC cell-scaffold constructs *in vivo*

Histological analysis of 8-week constructs with H&E staining shows that the very small-pore (60–125 μm, Figure 7A) scaffolds contained cartilage-like tissue in the center of the scaffold (light pink) with typical low cellularity and rounded hollow lacunae formation. The very smallpore scaffold underwent endochondral ossification only on the easily-vascularized edges of the scaffold (peripheral pink cellular bone matrix), thus explaining the observed significantly less bone volume (Figure 6A). The small, medium, and large pore scaffolds all

contained bone marrow-like tissue within the pores surrounded by bone tissue, consisting of: immune cells with darkly-stained nuclei, adipocytes (round, white spaces), and blood vessels filled with pink-stained red blood cells (Figure 7B-D). The well-interconnected, spherical pores retained their structure throughout and filled with marrow-containing bone after 8 weeks *in vivo*. Immunohistological staining of endothelial cell marker CD31 was performed to visualize blood vessel in-growth in the 8-week constructs (Figure 8). The cartilage in the very small pore scaffold remained essentially avascular (with some non-specific staining of the scaffold), while the blood vessels were formed inside the scaffolds with small, medium, and large-pore sizes. The in-grown blood vessels likely contributed to increased bone volume by carrying more oxygen, growth factors, other nutrients, and osteoprogenitor cells to enhance bone formation.

4. Discussion

4.1 Small-pore scaffolds support chondrogenesis both *in vitro* and *in vivo*.

Chondrogenesis is a tightly controlled developmental process, involving multiple steps [44]. Importantly, the phenotype of differentiated chondrocytes is dependent on the cell morphology. Chondrocytes often de-differentiate when cultured on a 2D surface as a monolayer and can re-differentiate in a rounded cell morphology after pellet [45, 46], transwell [47], hydrogel [48], or porous scaffold cultures [12, 49, 50]. Additionally, aggregation is critical to mimic the key mesenchymal condensation process. We hypothesized that the pore size of scaffolds can be used to affect the shape and aggregation of BMSCs, and subsequent chondrogenic commitment and differentiation. The experimental data demonstrates that the smaller pores enhanced chondrogenic differentiation (Figure 3), possibly due to a more rounded cell shape and increased aggregation, since the pore walls are more steeply curved (Figure 4).

This study showed that the small pores (125–250 μm) promoted chondrogenesis *in vitro*, with higher collagen type II and lower collagen type I gene expression levels, more GAG deposition, and more typical cartilage morphology including spherical cell shape and characteristic lacunae structure (Figure 4) [51]. Our gene expression and histological staining data corroborate to conclude that pore size plays an important role in determining BMSC fate. Following *in vivo* mouse subcutaneous implantation, small-pore scaffolds enhanced cartilage formation with GAG and collage type II matrix deposition (Figure 5). In contrast, large pore scaffolds allowed for vascular invasion, which facilitated vascularized bone formation. By preventing vessel ingrowth, thereby preventing vascularized bone formation, cartilage is formed in very small pore sized scaffolds. We believe that pore curvature may facilitate rounded cell shape and aggregation of BMSCs, plus create a more hypoxic environment, leading to our observation of chondrocyte-like cells [52, 53]. MSC plasticity is a known concern, and many studies demonstrate dedifferentiation phenomena, particularly from 3D to monolayer culture [54, 55]. Our small-pore scaffolds maintained the cartilage phenotype even after 8 weeks of subcutaneous implantation, following the four-week inductive in vitro culture period. These results corroborate with previous studies demonstrating the role of rounded 3D cell shape and extracellular matrix in maintaining chondrocyte phenotype [53, 56].

Previously, studies have reported that the chondrogenic differentiation is a function of cell density [57], so pore-size effects could be attributed to varied cell seeding efficiencies. However, in the current study the cell seeding efficiency was similar for small and large-pore scaffolds (Figure 2). It is noteworthy that the small-pore and large-pore scaffolds have different pore interconnection properties. Small and large-pore scaffolds have comparable interconnection opening to pore surface ratios (27.58 ± 7.38% for small-pore and 28.63 ± 8.27% for large-pore scaffolds, not significant, n=10) but differ in interconnection opening size (55.7 ± 14.41 μm for small-pore and 140.59 ± 26.60 μm for large-pore scaffolds, $p < 0.001$, n=10). Even very small pores are sufficient for cell seeding, migration, and nutrient exchange. We do not observe any significant difference in cell distribution inside the different pore size scaffolds, likely because our NF scaffolds are highly porous with a well-interconnected pore network (Figures 1 and 2). Prior to implantation to host animals, hBMSCs were cultured in scaffolds for 4 weeks of chondrogenic induction. The very small pore scaffold seeded with hBMSCs formed cartilage after 4 weeks in vitro but prevented blood vessel invasion in vivo and therefore prevented endochondral ossification (Figure 5A). Large-pore scaffold lead to low cartilage formation in vitro and allowed blood vessel penetration *in vivo* -- critical to the formation of vascularized bone (Figure 5B). Therefore, very small pore-size is an important factor in BMSC aggregation and subsequent chondrogenic differentiation; larger pore-sizes are critical to allow for vascularization and subsequent bone formation. Here we demonstrated a useful method for guiding cartilage-like or vascularized bone regeneration processes using the pore size of the macroporous NF scaffolds.

4.2 Endochondral ossification is prevented in very small pore-size scaffolds *in vivo*.

Endochondral ossification is the process by which a cartilaginous matrix is gradually replaced by bone and is important for bone healing. Blood vessel penetration into the cartilage template is a key step in successful endochondral ossification, requiring an internal porous network in a tissue engineering scaffold. Most previously reported scaffold systems require a pore size of 300 μm in order to allow capillary invasion for bone formation [14]. Impressively, the present study demonstrates that if the scaffold pores are well-interconnected, an even smaller pore-size scaffold (125–250 μm) supported mature bone formation (Figure 6). A pore-size less than 125 μm was required to prevent blood vessel ingrowth and inhibit endochondral ossification (Figure 7). Importantly, the very small pore scaffold (60–125 μm) still facilitated cell migration, due to the high pore interconnectivity, but instead promoted cartilage-like tissue formation because it could not support vascularization (Figure 8). Together data from microCT, hematoxylin and eosin histological staining, and CD31 immunohistochemistry corroborate to support that endochondral ossification is inhibited in very small pore scaffolds, and is enhanced in large pore scaffolds. Vascularization, evaluated by CD31 staining, is critical in aiding this process and determining BMSC osteogenic fate towards mineralized bone deposition. We conclude that scaffold pore size can control the endochondral ossification process by promoting or preventing host vasculature invasion.

Unlike many previous studies, cell-seeded scaffolds were implanted subcutaneously into nude mice one day after cell seeding for immediate interaction with host vasculature,

without any *in vitro* induction with soluble factors. This was possible because the early passage-3 rBMSCs were highly proliferative and could form a cartilage template in less than 3 weeks (data not shown), quickly laying the groundwork for successful endochondral ossification. After 8 weeks of subcutaneous implantation, our larger pore cell-scaffold constructs were filled with robust and mature bone, with bone-marrow like tissue (Figures 7 and 8).

We believe that our porous, nanofibrous poly (l-lactic acid) scaffold with uniform, spherical, highly interconnected pores provided a superior model for studying the effect of well-controlled pore size on chondrogenesis *in vitro* and endochondral ossification *in vivo*. Here we demonstrated that pore size is a critical scaffold design parameter to induce multiple BMSC differentiation fates through control of vascularization.

5. Conclusions

There is increasing recognition of the role of local microenvironment in stem cell differentiation [13]. As a result, the fields of biomaterials and tissue regeneration have made progress in designing microenvironments conducive to cell proliferation and differentiation, in an effort to engineer different tissues. Nanofibrous scaffolds are one such biomimetic approach shown to enhance bone and cartilage regeneration [12]. A phase-separated nanofibrous, macro-porous PLLA scaffold serves as a good model for this study due to: 1) a uniform, spherical, and well-interconnected pore architecture, and 2) nanofibers that promote cell proliferation and differentiation.

In the present study, scaffold pore size was used to control the highly-regulated processes of cartilage and bone formation by chondrogenesis and endochondral ossification, respectively. Nanofibrous PLLA scaffolds with a small pore size (125–250 μm) significantly enhanced chondrogenic differentiation of human BMSCs and cartilage formation compared to a large pore size (425–600 μm), both in vitro and in vivo (by controlling vascularization). We also demonstrated that a small pore size of 125–250 μm, even less than 300 μm, could still promote capillary ingrowth for mature bone formation in nanofibrous PLLA scaffolds seeded with rabbit BMSCs and implanted subcutaneously. Very small pore size scaffolds (60–125 μm) prevented endochondral ossification, while still allowing for cell migration and cartilage formation. Furthermore, larger pores supported mineralized bone tissue formation due to ingrowth of blood vessels through the pore network. We have demonstrates that modulating scaffold pore size allows for control of vascularization, which is a critical parameter in bone tissue engineering. Based on these positive results, we believe that tailoring the tunable pore architecture of nanofibrous polymer scaffolds may also improve the regeneration of many other tissue types.

Acknowledgements

The authors would like to acknowledge the following funding support: National Institutes of Health [Research Grants DE015384: PXM, DE017689: PXM, DE022327: PXM, HL114038: PXM, HL136231: PXM, S10RR026475–01: MicroCT Core, and Training Grant 5T32DE007057: MJG], US Department of Defense [W81XWH-12–2-0008: PXM], and National Science Foundation [DMR-1206575: PXM].

References

[1]. Hjelle K, Solheim E, Strand T, Muri R, Brittberg M, Articular cartilage defects in 1,000 knee arthroscopies, Arthroscopy-the Journal of Arthroscopic and Related Surgery 18(7) (2002) 730–734.

[2]. Matsusue Y, Yamamuro T, Hama H, Arthroscopic multiple osteochondral transplation to the chondral defect in the knee associated with anterior cruciate ligament disruption, Arthroscopy 9(3) (1993) 318–321. [PubMed: 8323618]

[3]. Mankin HJ, Reaction of articular-cartilage to injury and osteoarthritis. 2, New England Journal of Medicine 291(25) (1974) 1335–1340. [PubMed: 4610394]

[4]. Detterline AJ, Goldberg S, Bach BR, Jr., Cole BJ, Treatment Options for Articular Cartilage Defects of the Knee, Orthopaedic Nursing September/October 24(5) (2005) 361–366.

[5]. Hangody L, Fules P, Autologous osteochondral mosaicplasty for the treatment of fullthickness defects of weight-bearing joints - Ten years of experimental and clinical experience, Journal of Bone and Joint Surgery-American Volume 85A (2003) 25–32.

[6]. Langer R, Vacanti JP, Tissue Engineering, Science 260(5110) (1993) 920–926. [PubMed: 8493529]

[7]. Freed LE, Grande DA, Lingbin Z, Emmanual J, Marquis JC, Langer R, Joint resurfacing using allograft chondrocytes and synthetic biodegradable polymer scaffolds, J. Biomed. Mater. Res 28(8) (1994) 891–899. [PubMed: 7983087]

[8]. Ma P, Zhang R, Synthetic nano-scale fibrous extracellular matrix, J. Biomed. Mater. Res 46(1) (1999) 60–72. [PubMed: 10357136]

[9]. Ma PX, Biomimetic materials for tissue engineering, Adv Drug Deliv Rev 60(2) (2008) 184–98. [PubMed: 18045729]

[10]. Feng G, Jin X, Hu J, Ma H, Gupte MJ, Liu H, Ma PX, Effects of hypoxias and scaffold architecture on rabbit mesenchymal stem cell differentiation towards a nucleus pulposus-like phenotype, Biomaterials 32(32) (2011) 8182–8189. [PubMed: 21839506]

[11]. Hu J, Xie C, Ma H, Yang B, Ma PX, Chen YE, Construction of Vascular Tissues with Macro-Porous Nano-Fibrous Scaffolds and Smooth Muscle Cells Enriched from Differentiated Embryonic Stem Cells, PloS one 7(4) (2012).

[12]. Hu J, Feng K, Liu X, Ma P, Chondrogenic and osteogenic differentiations of human bone marrow-derived mesenchymal stem cells on a nanofibrous scaffold with designed pore network, Biomaterials 30(28) (2009) 5061–5067. [PubMed: 19564041]

[13]. Ma PX, Biomimetic materials for tissue engineering, Advanced Drug Delivery Reviews 60(2) (2008) 184–198. [PubMed: 18045729]

[14]. Karageorgiou V, Kaplan D, Porosity of 3D biornaterial scaffolds and osteogenesis, Biomaterials 26(27) (2005) 5474–5491. [PubMed: 15860204]

[15]. Conde CM, Demarco FF, Casagrande L, Alcazar JC, Nor JE, Tarquinio SB, Influence of poly-L-lactic acid scaffold's pore size on the proliferation and differentiation of dental pulp stem cells, Braz Dent J 26(2) (2015) 93–8. [PubMed: 25831096]

[16]. Tara S, Kurobe H, Rocco KA, Maxfield MW, Best CA, Yi T, Naito Y, Breuer CK, Shinoka T, Well-organized neointima of large-pore poly(L-lactic acid) vascular graft coated with poly(L-lactic-co-epsilon-caprolactone) prevents calcific deposition compared to small-pore electrospun poly(L-lactic acid) graft in a mouse aortic implantation model, Atherosclerosis 237(2) (2014) 684–91. [PubMed: 25463106]

[17]. Bruzauskaite I, Bironaite D, Bagdonas E, Bernotiene E, Scaffolds and cells for tissue regeneration: different scaffold pore sizes-different cell effects, Cytotechnology 68(3) (2016) 355–69. [PubMed: 26091616]

[18]. Brauker JH, Carr-Brendel VE, Martinson LA, Crudele J, Johnston WD, Johnson RC, Neovascularization of synthetic membranes directed by membrane microarchitecture, J Biomed Mater Res 29(12) (1995) 1517–24. [PubMed: 8600142]

[19]. Lim TC, Bang CP, Chian KS, Leong KF, Development of cryogenic prototyping for tissue engineering, Virtual and Physical Prototyping 3(1) (2008) 25–31.

[20]. Chiu YC, Cheng MH, Engel H, Kao SW, Larson JC, Gupta S, Brey EM, The role of pore size on vascularization and tissue remodeling in PEG hydrogels, Biomaterials 32(26) (2011) 6045–51. [PubMed: 21663958]

[21]. Ma PX, Choi JW, Biodegradable polymer scaffolds with well-defined interconnected spherical pore network, Tissue Engineering 7(1) (2001) 23–33. [PubMed: 11224921]

[22]. Ikada Y, Scope of Tissue Engineering, Tissue Engineering: Fundamentals and Applications 2006, pp. 1–89.

[23]. Lu JX, Flautre B, Anselme K, Hardouin P, Gallur A, Descamps M, Thierry B, Role of interconnections in porous bioceramics on bone recolonization in vitro and in vivo, Journal of Materials Science-Materials in Medicine 10(2) (1999) 111–120. [PubMed: 15347932]

[24]. Mastrogiacomo M, Scaglione S, Martinetti R, Dolcini L, Beltrame F, Cancedda R, Quarto R, Role of scaffold internal structure on in vivo bone formation in macroporous calcium phosphate bioceramics, Biomaterials 27(17) (2006) 3230–3237. [PubMed: 16488007]

[25]. Offeddu GS, Ashworth JC, Cameron RE, Oyen ML, Multi-scale mechanical response of freeze-dried collagen scaffolds for tissue engineering applications, J Mech Behav Biomed Mater 42 (2015) 19–25. [PubMed: 25460922]

[26]. Murphy WL, Dennis RG, Kileny JL, Mooney DJ, Salt fusion: an approach to improve pore interconnectivity within tissue engineering scaffolds, Tissue Eng 8(1) (2002) 43–52. [PubMed: 11886653]

[27]. Wei GB, Ma PX, Macroporous and nanofibrous polymer scaffolds and polymer/bone-like apatite composite scaffolds generated by sugar spheres, Journal of Biomedical Materials Research Part A 78A(2) (2006) 306–315.

[28]. Liu X, Jin X, Ma PX, Nanofibrous hollow microspheres self-assembled from star-shaped polymers as injectable cell carriers for knee repair, Nature Materials 10(5) (2011) 398–406. [PubMed: 21499313]

[29]. Jones JR, Poologasundarampillai G, Atwood RC, Bernard D, Lee PD, Non-destructive quantitative 3D analysis for the optimisation of tissue scaffolds, Biomaterials 28(7) (2007) 1404–13. [PubMed: 17141863]

[30]. Mano JF, Reis RL, Osteochondral defects: present situation and tissue engineering approaches, Journal of Tissue Engineering and Regenerative Medicine 1(4) (2007) 261–273. [PubMed: 18038416]

[31]. Klein TJ, Malda J, Sah RL, Hutmacher DW, Tissue Engineering of Articular Cartilage with Biomimetic Zones, Tissue Engineering Part B-Reviews 15(2) (2009) 143–157. [PubMed: 19203206]

[32]. Woods A, Wang G, Beier F, Regulation of chondrocyte differentiation by the actin cytoskeleton and adhesive interactions, J Cell Physiol 213(1) (2007) 1–8. [PubMed: 17492773]

[33]. Winter A, Breit S, Parsch D, Benz K, Steck E, Hauner H, Weber RM, Ewerbeck V, Richter W, Cartilage-like gene expression in differentiated human stem cell spheroids: a comparison of bone marrow-derived and adipose tissue-derived stromal cells, Arthritis Rheum 48(2) (2003) 418–29. [PubMed: 12571852]

[34]. Salinas CN, Anseth KS, The enhancement of chondrogenic differentiation of human mesenchymal stem cells by enzymatically regulated RGD functionalities, Biomaterials 29(15) (2008) 2370–2377. [PubMed: 18295878]

[35]. Gerber HP, Vu TH, Ryan AM, Kowalski J, Werb Z, Ferrara N, VEGF couples hypertrophic cartilage remodeling, ossification and angiogenesis during endochondral bone formation, Nature Medicine 5(6) (1999) 623–628.

[36]. Boyde A, Corsi A, Quarto R, Cancedda R, Bianco P, Osteoconduction in large macroporous hydroxyapatite ceramic implants: Evidence for a complementary integration and disintegration mechanism, Bone 24(6) (1999) 579–589. [PubMed: 10375200]

[37]. Chang BS, Lee CK, Hong KS, Youn HJ, Ryu HS, Chung SS, Park KW, Osteoconduction at porous hydroxyapatite with various pore configurations, Biomaterials 21(12) (2000) 1291–1298. [PubMed: 10811311]

[38]. Smith LA, Liu XH, Hu JA, Ma PX, The Enhancement of human embryonic stem cell osteogenic differentiation with nano-fibrous scaffolding, Biomaterials 31(21) (2010) 5526–5535. [PubMed: 20430439]

[39]. Liu X, Jin X, Ma PX, Nanofibrous hollow microspheres self-assembled from star-shaped polymers as injectable cell carriers for knee repair, Nat Mater 10(5) (2011) 398–406. [PubMed: 21499313]

[40]. Liu XH, Ma PX, Polymeric scaffolds for bone tissue engineering, Annals of Biomedical Engineering 32(3) (2004) 477–486. [PubMed: 15095822]

[41]. Wu LB, Ding JD, Effects of porosity and pore size on in vitro degradation of threedimensional porous poly(D,L-lactide-co-glycolide) scaffolds for tissue engineering, Journal of Biomedical Materials Research Part A 75A(4) (2005) 767–777.

[42]. Hu DP, Ferro F, Yang F, Taylor AJ, Chang W, Miclau T, Marcucio RS, Bahney CS, Cartilage to bone transformation during fracture healing is coordinated by the invading vasculature and induction of the core pluripotency genes, Development 144(2) (2017) 221–234. [PubMed: 28096214]

[43]. Farndale RW, Sayers CA, Barrett AJ, A Direct Spectrophotometric Micro-Assay for Sulfated Glycosaminoglycans in Cartilage Cultures, Connective Tissue Research 9(4) (1982) 247–248. [PubMed: 6215207]

[44]. Goldring MB, Tsuchimochi K, Ijiri K, The control of chondrogenesis, Journal of Cellular Biochemistry 97(1) (2006) 33–44. [PubMed: 16215986]

[45]. Mackay AM, Beck SC, Murphy JM, Barry FP, Chichester CO, Pittenger MF, Chondrogenic differentiation of cultured human mesenchymal stem cells from marrow, Tissue Engineering 4(4) (1998) 415–428. [PubMed: 9916173]

[46]. Pittenger MF, Mackay AM, Beck SC, Jaiswal RK, Douglas R, Mosca JD, Moorman MA, Simonetti DW, Craig S, Marshak DR, Multilineage potential of adult human mesenchymal stem cells, Science 284(5411) (1999) 143–147. [PubMed: 10102814]

[47]. Murdoch AD, Grady LM, Ablett MP, Katopodi T, Meadows RS, Hardingham TE, Chondrogenic differentiation of human bone marrow stem cells in transwell cultures: Generation of Scaffold-free cartilage, Stem Cells 25(11) (2007) 2786–2796. [PubMed: 17656642]

[48]. Elisseeff J, McIntosh W, Anseth K, Riley S, Ragan P, Langer R, Photoencapsulation of chondrocytes in poly(ethylene oxide)-based semi-interpenetrating networks, J. Biomed. Mater. Res 51(2) (2000) 164–171. [PubMed: 10825215]

[49]. Freed LE, Marquis JC, Nohria A, Emmanual J, Mikos AG, Langer R, Neocartilage formation in vitro and in vivo using cells cultured on synthetic biodegradable polymers, J Biomed Mater Res 27(1) (1993) 11–23. [PubMed: 8380593]

[50]. Li WJ, Tuli R, Okafor C, Derfoul A, Danielson KG, Hall DJ, Tuan RS, A three-dimensional nanofibrous scaffold for cartilage tissue engineering using human mesenchymal stem cells, Biomaterials 26(6) (2005) 599–609. [PubMed: 15282138]

[51]. Benya PD, Padilla SR, Nimni ME, Independent regulation of collagen types by chondrocytes during the loss of differentiated function in culture, Cell 15(4) (1978) 1313–21. [PubMed: 729001]

[52]. Adesida AB, Mulet-Sierra A, Jomha NM, Hypoxia mediated isolation and expansion enhances the chondrogenic capacity of bone marrow mesenchymal stromal cells, Stem Cell Res Ther 3(2) (2012) 9. [PubMed: 22385573]

[53]. Benya PD, Shaffer JD, Dedifferentiated chondrocytes reexpress the differentiated collagen phenotype when cultured in agarose gels, Cell 30(1) (1982) 215–24. [PubMed: 7127471]

[54]. Grove JE, Bruscia E, Krause DS, Plasticity of bone marrow-derived stem cells, Stem Cells 22(4) (2004) 487–500. [PubMed: 15277695]

[55]. Oreffo RO, Cooper C, Mason C, Clements M, Mesenchymal stem cells: lineage, plasticity, and skeletal therapeutic potential, Stem Cell Rev 1(2) (2005) 169–78. [PubMed: 17142852]

[56]. Benya PD, Nimni ME, The stability of the collagen phenotype during stimulated collagen, glycosaminoglycan, and DNA synthesis by articular cartilage organ cultures, Arch Biochem Biophys 192(2) (1979) 327–35. [PubMed: 434828]

[57]. Vunjak-Novakovic G, Obradovic B, Martin I, Bursac PM, Langer R, Freed LE, Dynamic cell seeding of polymer scaffolds for cartilage tissue engineering, Biotechnology Progress 14(2) (1998) 193–202. [PubMed: 9548769]

Statement of Significance

Progress in understanding the relationship between cell fate and architectural features of tissue engineering scaffolds is critical for engineering physiologically functional tissues. Sugar porogen template scaffolds have uniform, spherical, highly interconnected macropores. Tunable pore-size guides the fate of bone marrow stromal cells (BMSCs) towards chondrogenesis and endochondral ossification, and is a critical design parameter to mediate neotissue vascularization. Preventing vascularization favors a chondrogenic cell fate while allowing vascularization results in endochondral ossification and mineralized bone formation. These results provide a novel strategy to control tissue regenerative processes by tunable architecture of macroporous nanofibrous scaffolds.

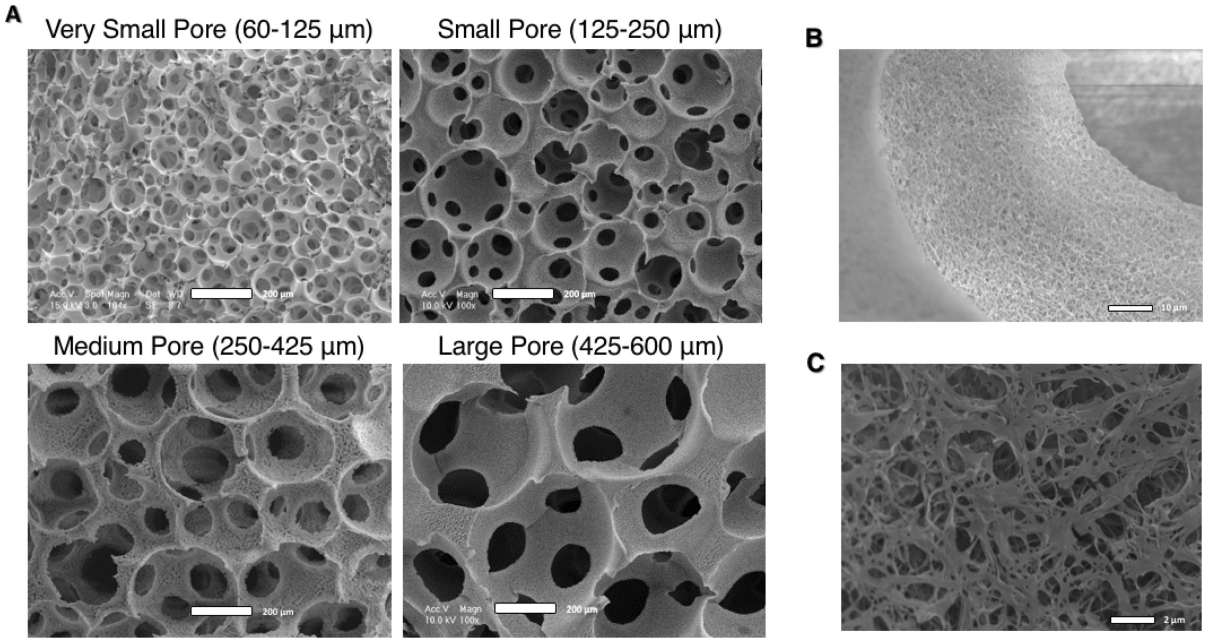

Figure 1.

SEM Micrographs of nanofibrous PLLA scaffolds of four distinct pore size ranges with uniform, spherical, well-interconnected macro-pores (A, scale bar = 200 µm). At higher magnification, the nanofibrous microstructure of the pore walls is apparent (B, scale bar = 10 µm), and an appreciation for their biomimetic diameter is apparent at even higher magnification (C, scale bar = 2 µm).

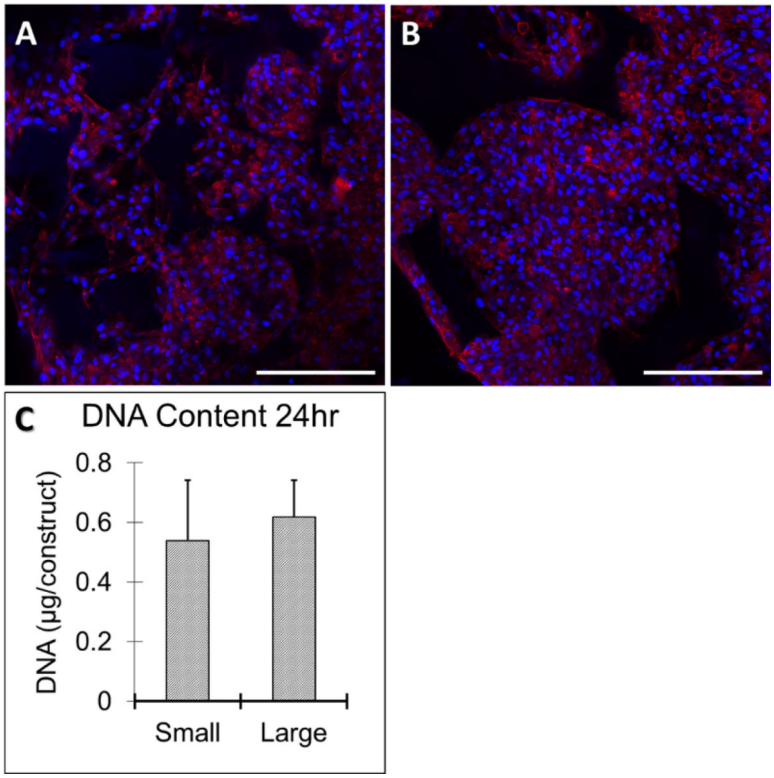

Figure 2.

Human bone marrow stromal cells (hBMSCs) adhered to and aggregated within small (125–250 μm) (A) and large pore (425–600 μm) (B) scaffolds 24 hours after seeding, shown by immunofluorescent staining of F-actin (red) and nuclei (blue). Scale bar: 200 μm. There was no significant difference in cell-seeding efficiency between the two pore sizes, demonstrated by quantification of total DNA amount (C). n=3 for each group. Scale bars = 100 μm.

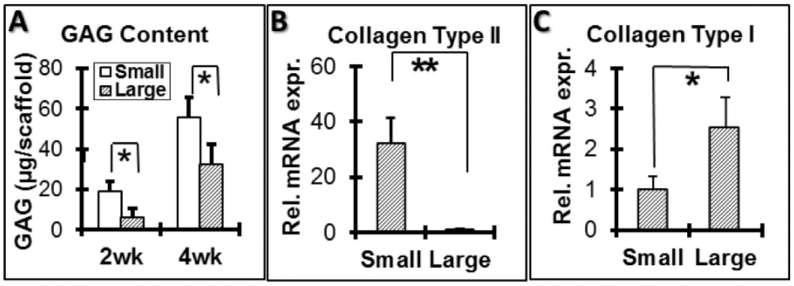

Figure 3.

Glycosaminoglycan (GAG) quantification and gene expression of hMSCs seeded on small (125–250 μm) and large-pore (425–600 μm) scaffolds during *in vitro* chondrogenic culture with 10 ng/mL TGF-β1. Small-pore scaffolds had significantly higher GAG content per scaffold at both 2 and 4 weeks of culture (A). Small-pore scaffolds also had significantly higher collagen type II gene expression (B) and significantly lower collagen type I gene expression (C) after 2 weeks of culture. *$p<0.05$; **$p<0.01$. n=3 for each group. Scale bars = 100 μm.

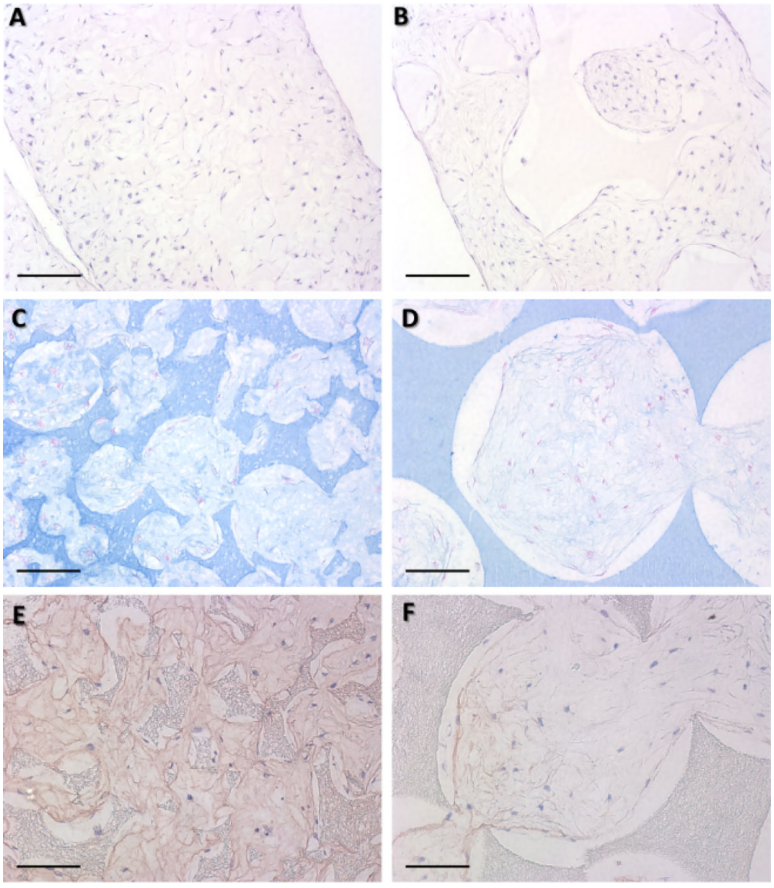

Figure 4.

Histological analyses at 4 weeks *in vitro* chondrogenic culture of hMSCs on small and large-pore scaffolds. H&E staining shows that cells grew throughout the whols scaffolds in both small (125–250 μm) (A) and large-pore (425–600 μm) (B) scaffolds (Scale bar: 200 μm). Alician blue staining showed a denser glycosaminoglycan matrix deposition in small (C) as compared to large-pore (D) scaffolds (Scale bar: 100 μm). Similarly, collagen type II immunohistochemical staining revealed more collaged type II matrix deposition in small (E) than large-pore (F) scaffolds (Scale bar: 100 μm). n=3 for each group.

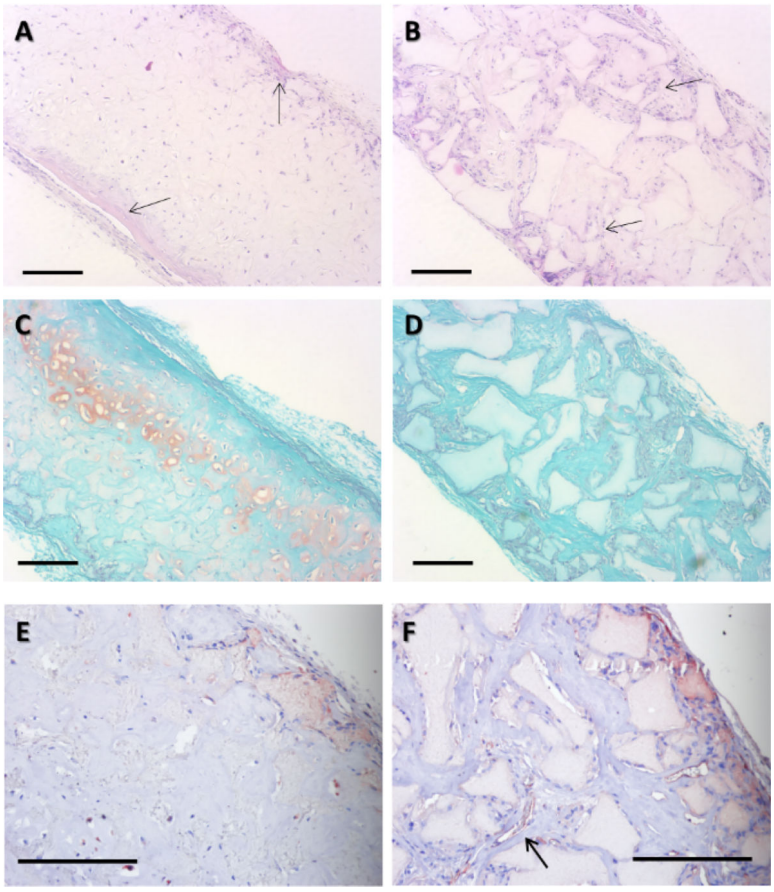

Figure 5.

H&E, Safranin-O, and CD31 staining following 4 wk *in vitro* chondrogenic culture and 8 wk subcutaneous implantation in nude mice. H&E staining revealed that small-pore (125–250 *μm*) implants had typical cartilage morphology (A) with moderate ectopic bone formation (arrows) on scaffold surface. Large-pore (425–600 *μm*) implants show blood vessel ingrowth (B), preventing maintenance of a chondrogenic phenotype. Safranin-O staining showed that smallpore implants was positive for GAG-containing matrix (C), whereas large-pore implants were negative (D). CD31 immunohistochemical staining for endothelial cells showed that small-pore implants were mostly avascular (E), but large-pore implants contained rich microvessels (F, arrow indicates a typical microvessel). Scale bar: 200 *μm*. n=3 for each group.

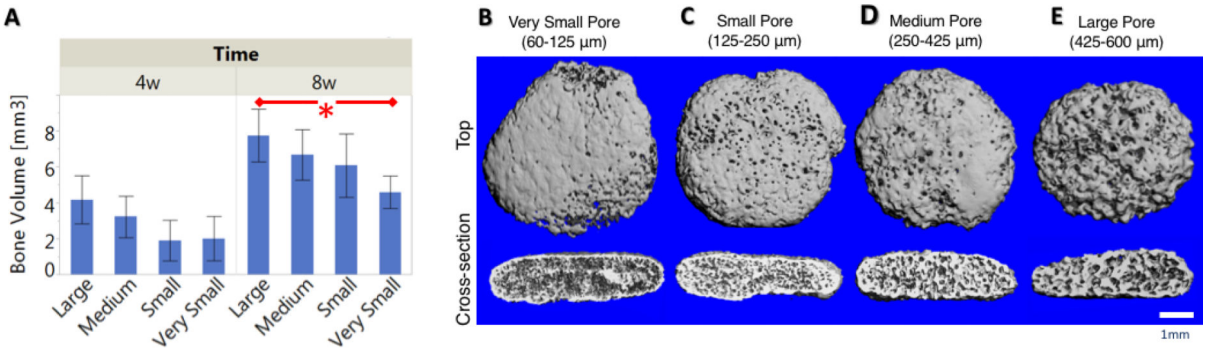

Figure 6.

Bone volume quantification from MicroCT analysis after 4 or 8 weeks subcutaneous implantation of large (425–600 μm), medium (250–425 μm), small (125–250 μm), and very small (60–125 μm) pore size scaffolds (A). Small, medium, and large pore scaffolds supported robust bone formation after 8 weeks. Very small scaffolds inhibited bone formation and had significantly less bone volume than large pore scaffold (*$p<0.05$). MicroCT 3D reconstructions of four different pore size scaffolds (B-E) after 8 weeks mouse subcutaneous implantation from top view and side cross-section. Very small pore scaffold (60–125 μm, B) exhibited bone formation mainly on the outer surface of the scaffold. Small, medium, and large pore scaffolds supported robust, uniform bone formation throughout cross section. n=3 for each group. Scale bar = 1 mm.

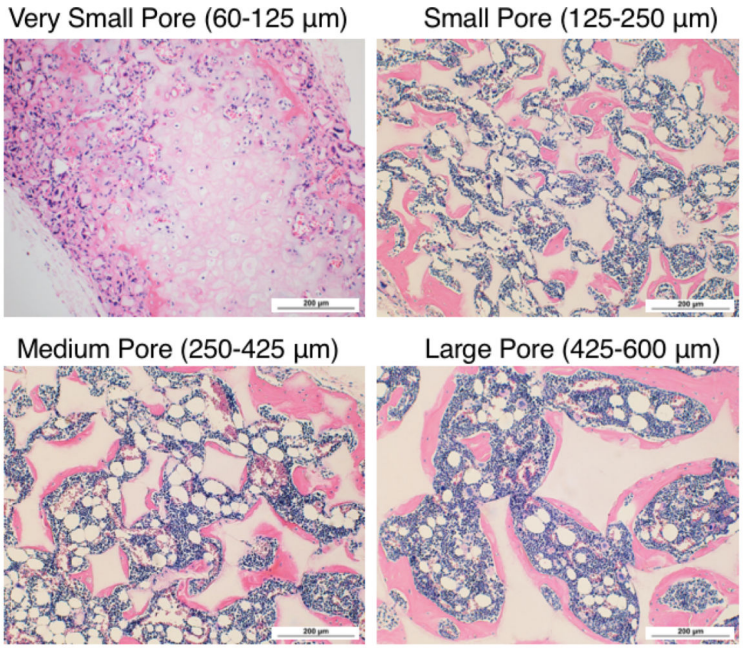

Figure 7.

H&E histological analysis after 8 weeks subcutaneous implantation at 100× magnification. Very small pore scaffold (60–125 μm, A) contained cartilage with typical morphology in the center of the scaffold. Small (125–250 μm, B), medium (250–425 μm, C), and large-pore (425–600 μm, D) scaffolds supported bone formation on pore walls, shown by pink staining of bone matrix, with bone marrow-like tissue within the pores. n=3 for each group. Scale bars = 200 μm.

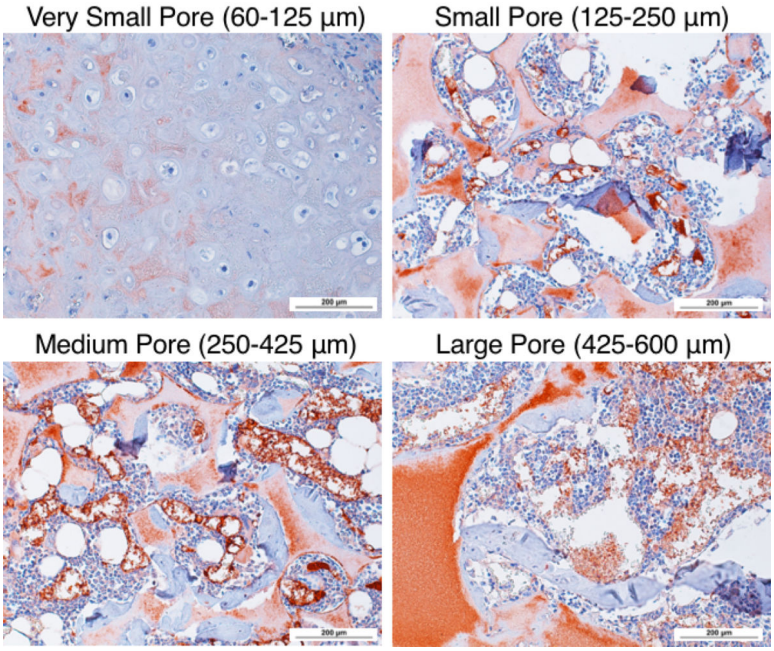

Figure 8.

CD31 immunohistochemical staining of endothelial layer and visualization of blood cells at 200× magnification as red-brown. Cartilage in very small pore scaffold is avascular. Blood vessels within small, medium, and large pore scaffold increase in size within increasing pore size. Note that the scaffold also stains red due to the high surface area of the nanofibers. n=3 for each group. Scale bar = 200 μm.